Split Ring Resonator Antenna System with Cortical Implant and Head-worn Parts for Effective Far Field Implant Communications

Shubin Ma (马述彬), *Student Member, IEEE,* Lauri Sydänheimo, *Member, IEEE,*
Leena Ukkonen, *Member, IEEE, and Toni Björninen, Member, IEEE*

***Abstract*—We propose a spatially distributed antenna system to serve as the radio platform for RFID inspired brain care applications. The antenna system consists of a passive wearable part placed on the scalp and a cortical implant part with split ring resonator topology for miniaturization and antenna self-matching with a backscattering microsystem. We have optimized the antenna system in a hybrid head model combining anatomical features with a layered ellipsoid mimicking the major tissue layers of the human head in a controlled manner. Results from the wireless testing of the prototyped antenna system indicate that it enables remote powering and readout of a −18 dBm RFID microsystem at a distance of one meter at 915 MHz with 10 mm implant depth. Moreover, our experiment shows that the studied system is tolerant toward misalignment between the implantable and wearable parts.**

***Index Terms*—Split ring antenna, electro-textile, wearable antenna, implantable antenna, RFID**

INTRODUCTION

Wireless implantable sensors for intracranial signal (e.g. ECoG and intracranial pressure) extraction are believed to possess promises for brain diseases treatment and quality of life improvement for the patients suffering from a traumatic brain or spinal cord injury or stroke [1]. One of the major challenges when deploying such wireless implantable system is achieving a reliable wireless radio link inside and around human head due to the structural complexity and unfavorable electromagnetic properties of the biological environment. For this reason, various human tissue models with different complexity and modeling approaches have been proposed to predict the behavior of electromagnetic wave in the proximity of the human head [2], [3]. Meanwhile, the miniaturization requirement of the implant to reduce the patient's risk of tissue scarring also adds difficulty to the overall design of an implantable sensor. In a sensor with a miniature size, battery is no longer an optimal power source and remote powering of the system becomes preferable. RFID based sensors are thus proposed. Equipped with RFID technology, the sensor can harvest energy through the near-field electromagnetic field generated by an off-body device and send back the sampled data via a backscattering radio link. Without the necessity of the battery, the sensor footprint is largely decreased and the miniaturization of its antenna system becomes especially important.

According to a recent literature survey [4], planar inverted-F antenna (PIFA) is the most common approach to achieve small implantable antennas. However, it requires a ground plane and sometimes, additional vias and interconnected metallization layers have been introduced for the purpose of miniaturization. Therefore, it is hard to achieve thin and flexible structure and in [4] all of the reviewed antennas comprise rigid circuit boards. To provide an alternative approach, we have proposed a spatially distributed antenna shown in Fig. 1 [5]. In this approach, only a thin and flexible split ring resonator (SRR) inspired part is implanted and for far field performance boost, a wearable part is affixed on the skin. In this approach, where we only implant part of the antenna and also avoid the challenging task of downsizing the whole antenna structure as the size of the wearable part is not as strictly limited in this application.

In this article, we will further investigate the implementation of a radio platform for brain care applications based on the SRR inspired antenna system shown in Fig. 1. We introduce a layered ellipsoid model for the human head to assess the system's performance in a realistic setting compared with [5] and present further experimental evaluations of the robustness of the antenna system toward misalignment between the two parts. Finally, we verify the electromagnetic performance of the system when the wearable part is made of textile conductor.

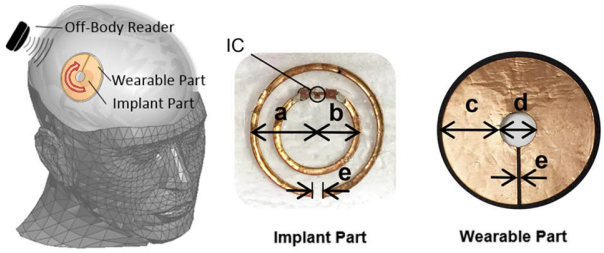

Geometrical parameter (mm)	a	b	c	d	e
	8.6	5.7	20.8	12.6	1.0

Fig. 1. Ellipsoid head model and prototyped antenna system with its geometrical dimensions.

This research work is funded by Academy of Finland, Jane and Aatos Erkko Foundation and Finnish Funding Agency for Technology and Innovation (TEKES).

The authors are with BioMediTech Institute and Faculty of Biomedical Science and Engineering, Tampere University of Technology, Tampere, Finland (e-mail: {shubin.ma, leena.ukkonen, lauri.sydanheimo, toni.bjorninen}@tut.fi).

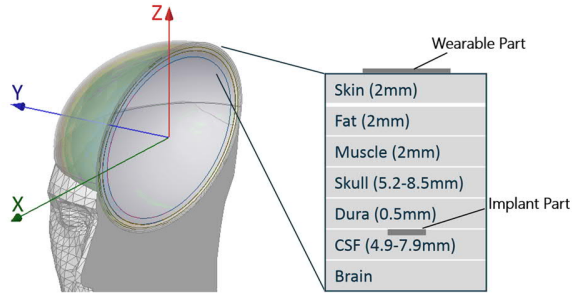

Fig. 2. Anatomical human head model with the layered ellipsoid.

ANTENNA DEVELOPMENT

Fig. 1 illustrates the fabricated RFID antenna system with its geometrical dimensions and the implemented position in the ellipsoid head model. We made the implant part with two concentric 35 µm thick copper (σ = 58 MS/m) rings. The 50 µm thick flexible polyethylene (ε_r = 2.25, tanδ = 0.001 at 915 MHz) was used as the substrates. We attached the NXP UCODE G2iL series RFID IC to the inner ring split of the implant part using Circuit Works CW2400 conductive epoxy. We made a 1 mm thick coating box with silicone (ε_r = 2.2, tanδ = 0.007 at 915 MHz) wrapping the implant to isolate the conductor from human tissue. The wearable part inspired by the triple split-ring structure is affixed to the skin with its slit on the same direction as that of the outer ring of the implant part. We made it with the same 35 µm thick copper foil with 2 mm thick EPDM (Ethylene-Propylene-Diene-Monomer; ε_r = 1.26, tanδ = 0.007 at 915 MHz) as the substrate.

A. Simulation Model

All the electromagnetic modeling and simulation were conducted in ANSYS High Frequency Structure Simulator (HFSS). In the simulation, we used the parallel connection of the resistance and capacitance of 2.85 kΩ and 0.91 pF, respectively, to model the RFID IC [6]. Meanwhile, we adopted the ANSYS anatomical human head model and built a seven-layer ellipsoid to mimic the human head including the most important tissue types. Fig. 2 shows the details of the anatomical head model combined with the layered ellipsoid. The ellipsoid was constructed by fitting its shape to the anatomical head model by visual inspection and then building the seven tissue layers, namely skin, fat, muscle, skull, dura, CSF (cerebrospinal fluid) and brain, which are the major tissue layers of the human head in terms of thickness. The thicknesses of skin, fat, muscle layers were selected according to [7]. The thickness of dura layer was set to 0.5 mm, which is close to the median of 0.3 mm – 0.8 mm [8]. In reality, the skull thickness and the width of the subarachnoid space (SAS) occupied by CSF vary greatly depending on the location. Therefore, we measured these values over several cross-sectional slices of the anatomical head model to obtain averaged values. The thinner regions of the skull tend to coincide with wider SAS. Moreover, since we consider attaching the implant to the dura (Fig. 2), the range for the skull thickness we present in Fig. 2 is the mean minimum thickness, whereas the CSF layer thickness is the mean maximum SAS width. This selection was made because we considered its benefits for both safety and wireless performance to maximize/minimize the distance between the implant and the brain/wearable part. In the simulation, all the tissues were assigned with their corresponding relative permittivity and loss tangent according to the frequency dependent four-term Cole-Cole relaxation model [9]. The database of tissue properties utilized in this work is obtained from IT'IS Foundation [10].

Despite the fact that the ellipsoid model can be readily built in the simulator, in practice it is very hard to create a solid phantom with exactly the same shape and tightly controlled tissue layer thickness and dielectric properties. Therefore, in the testing, we used a homogeneous liquid phantom in a container having the shape of a truncated cone (lower radius: 6.75 cm, upper radius: 8.25 cm, height: 8 cm). The head equivalent liquid was made with 42% of water, 57% of sugar and 1% of salt having the dielectric properties of ε_r = 41.5, σ = 0.98 S/m at 915 MHz [11]. For the comparison between the measurement and simulations, we implemented exactly the same model also in the simulator.

B. Antenna Optimization

In the passive UHF RFID system, RFID tag communicates with the reader by impedance modulated backscattering radio link. Since the RFID readers have typically high sensitivity of –70dB…–90dB, the maximum detectable distance of the tag is determined by the distance at which the tag could absorb enough power to exceed the wake up power threshold of the RFID IC. Friis' free-space formula can be used to calculate this maximum off-body detectable distance d_{tag} as

$$d_{tag} = \frac{\lambda}{4\pi}\sqrt{\frac{De_r\tau EIRP}{P_{ic0}}} \tag{1}$$

where D is the antenna directivity, e_r is the radiation efficiency, P_{ic0} is the RFID IC wake-up power threshold and τ is the power transfer efficiency given by

$$\tau = \frac{4\mathrm{Re}(Z_A)\mathrm{Re}(Z_c)}{|Z_A+Z_C|^2} \tag{2}$$

where Z_A is the antenna impedance and Z_C is IC impedance. Power transfer efficiency measures the ratio between the power available from the tag antenna to that transferred to IC. It reaches the maximum value when the antenna and IC are complex-conjugate matched with each other.

According to (1), the tag read range is in direct proportion to antenna gain and power transfer efficiency. Thus, in the optimization of the geometrical dimensions of the antenna, we targeted at both good complex-conjugate impedance matching with the IC and a high antenna gain. We found that the wearable part had negligible influence on the antenna impedance and thus were able to achieve the impedance matching by optimization of the geometrical dimensions of the implant part independent from those of the wearable part. As shown in Fig. 3, complex-conjugate impedance matching is closest at 915 MHz. Despite the difference in real parts of the antenna and IC impedances, τ reaches 70% at 915 MHz.

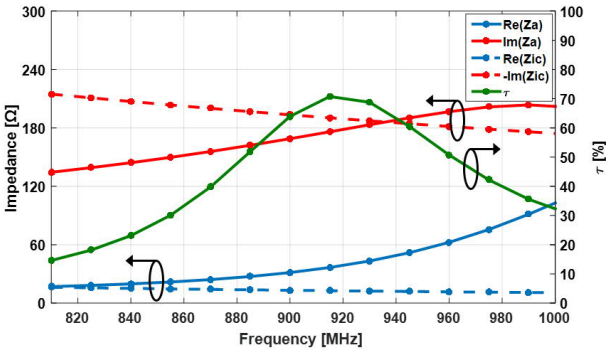

Fig. 3. Antenna impedance, complex-conjugate of the IC impedance, and the antenna-IC power transfer efficiency.

The geometrical dimensions of the wearable part were optimized to maximize the system directivity. According to the simulation results, the antenna directivity increased by 8 dB reaching 4.3 dBi with the wearable part concentrically placed 10 mm away from the implant part. Meanwhile, the simulated radiation efficiency is 0.48%.

In the ellipsoid model, the thicknesses of skull layers were set to its smallest value 5.2 mm and thus the implant depth was 11.7 mm. To compare the results from the two models, we set the same 11.7 mm implant depth in the liquid phantom model. Fig. 4 shows the simulated read range from the two models and they give similar results with slightly different frequency of the peak value. In general, the proposed antenna system is capable of providing 0.8 m attainable read range within the 902…928 MHz band.

Results From Wireless Testing

We tested the prototyped antenna system with Voyantic Tagformance measurement system in an anechoic chamber. Fig. 5 demonstrates the measurement setup. It consists of the reader antenna, the RFID measurement unit with an adjustable transmission frequency from 600 MHz to 1.2 GHz with up to 30 dBm output power and the control software. The system is capable of detecting the backscattering signal strengths down to −80 dBm. During the measurement, we first characterized the wireless channel between the measurement system and the AUT with a system reference tag with known properties. Then the lowest continuous transmission power to ensure the receiving of the response to the query command from the reader

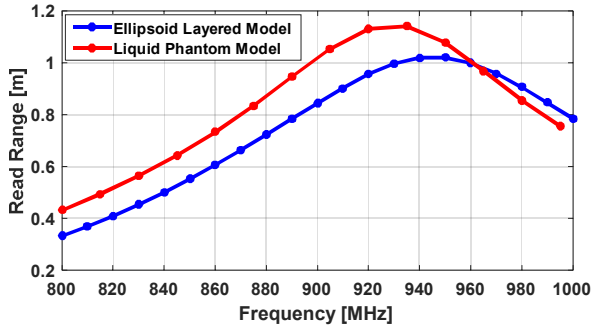

Fig. 4. Comparison of the simulated read range of the ellipsoid layered model and liquid phantom model.

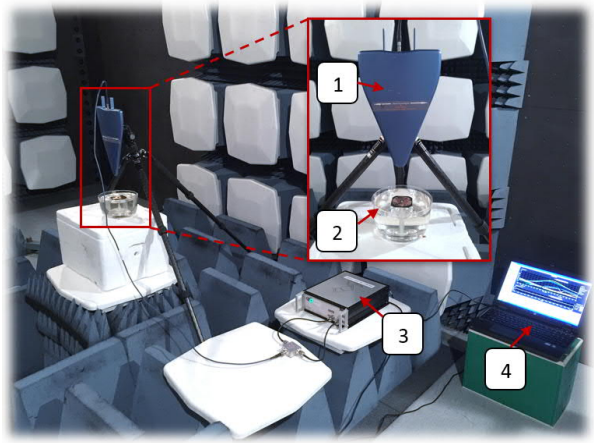

Fig. 5. Wireless Measurement setup 1: Reader antenna 2: Liquid phantom with antenna system under test 3: Tagformance measurement unit 4: Control software.

was recorded as P_{th}. With the measured output threshold power of the reference tag P_{th*}, the system sensitivity constant Λ and the emission power limit of the measurement system *EIRP*, the attainable read range of the tag versus frequency can be calculated by [12],

$$d_{tag} = \frac{\lambda}{4\pi}\sqrt{\frac{EIRP}{\Lambda}\frac{P_{th}^{*}}{P_{th}}} \tag{3}$$

The head equivalent liquid made with water, sugar and salt was used to mimic the human tissue environment in wireless measurement. Its relative permittivity and conductivity were confirmed with Agilent Technologies 85070E Dielectric Probe.

In the wireless measurement, the implant part was submerged in the liquid at three different implant depths: 5 mm, 10 mm and 15 mm. Fig. 6 shows the comparison between the measured read range and the simulated read ranges from the homogeneous truncated cone model. A good match was found especially in 5 mm and 10 mm cases. In the 15 mm case, the measured read range was higher than the simulated one from the simulation.

A. Misalignments Test

In order to investigate the antenna system sensibility to the misalignment between the two parts. We also tested the read range with lateral and rotational misalignment between the wearable and implantable parts. In the lateral misalignment test,

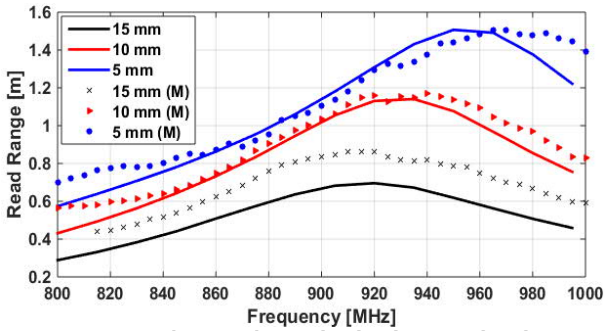

Fig. 6. Comparison between the simulated and measured read range at three different implant depths.

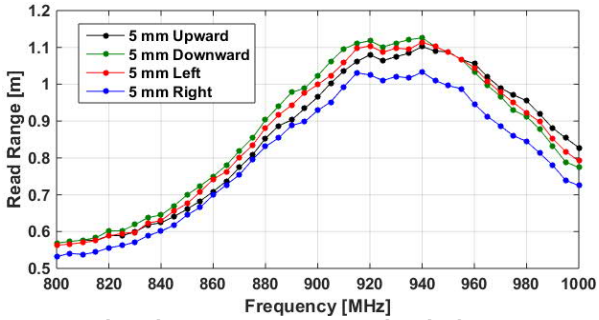

Fig. 7. Lateral misalignment test at 10 mm implant depth.

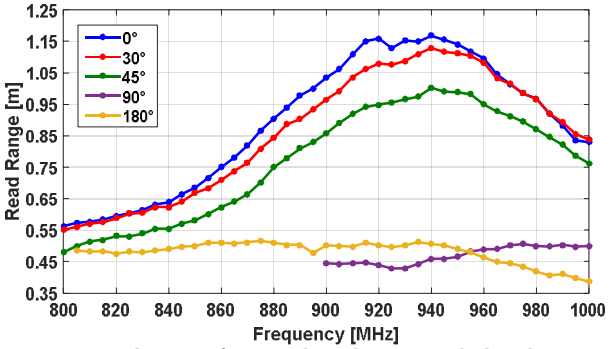

Fig. 8. Measured impact of rotational misalignment in the liquid phantom at 10 mm implant depth.

the wearable part was moved 5 mm from the central position to four different directions with the implant part fixed in the liquid. In the rotational misalignment test, the wearable part was rotated clockwise from 0° to 180° as shown by the arrow in Fig.1. Fig. 7 shows the measured read range in the lateral misalignment test, in the four directions of the misalignment the read range maintains at a very similar level with less than 0.1 m deviation compared with the non-misalignment situation. Fig. 8 compares the read range with different rotational misalignments. The read range dropped with the increase of the rotational misalignment from 0° to 90°. When the misalignment angle was larger than 90°, the backscattered signal was too weak to be detected. However, a nearly 0.5 m read range was measured when the wearable part rotated 180° through the whole UHF band.

B. Conductive Textile

To improve the flexibility and durability of the wearable part, we fabricated also an e-textile version of it with Less EMF Shieldit Super™ conductive textile featuring a sheet resistance less than 0.5 Ohm/m^2 and EPDM as the substrate. According to the results from the wireless measurement in Fig. 9, the e-textile version has very similar performance compared with the copper one. This adds further assurance to the practical implementation where the user's comfort is a pertinent aspect.

CONCLUSIONS

To face the challenge of establishing the radio link for the implantable wireless brain care application, we developed a spatially distributed passive UHF antenna system with an SRR inspired implant part and an inductive coupled wearable part.

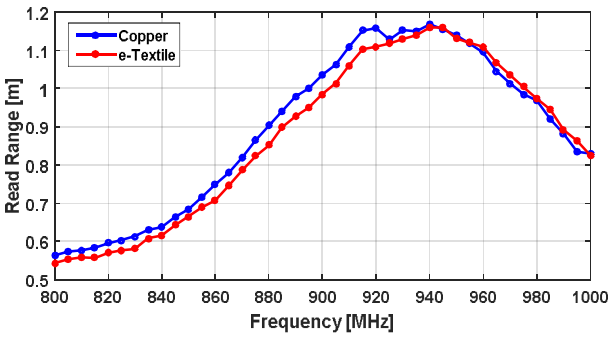

Fig. 9. Comparison of measured read range of copper and conductive fabric wearable part at 10 mm implant depth

By adopting the SRR topology, the implant part is downsized to $\pi \times 8.6^2 \times 1$ mm^3 and the antenna impedance is complex-conjugate matched with the capacitive RFID IC without any matching components. In the wireless measurement with liquid mimicking human head environment, the prototyped antenna system was verified to provide up to 1.1 m backscattering read range at 10 mm implant depth even with moderate lateral or rotational misalignments between the implantable and wearable parts. Our future work will focus on integrating physiological sensors into the presented antenna system.

REFERENCES

[1] M. O. Krucoff *et al.*, "Enhancing nervous system recovery through neurobiologics, neural interface training, and neurorehabilitation," *Front. Neurosci.*, vol. 10, no. 584, p. 23, Dec. 2016.

[2] L. Zhao *et al.*, "A new high-resolution electromagnetic human head model," *IEEE Antennas Propag. Mag.*, no. 5, pp. 32-42, Oct. 2016.

[3] S. Mustafa *et al.*, "Modeling human head tissues using fourth-order Debye model in convolution-based three-dimensional finite-difference time-domain," *IEEE Trans. Antennas Propag.*, vol. 62, no. 3, pp. 1354–1361, Jan. 2014.

[4] C. Liu *et al.*, "A review of implantable antennas for wireless biomedical devices," in *Forum Electromagn. Res. Methods Appl. Technol.*, vol. 14, no. 2, 2016.

[5] Shubin Ma *et al.*, "Split ring resonator antenna system with implantable and wearable parts for far field readable backscattering implants," in *Proc. IEEE AP Soc. Intl. Symp. on Antennas and Propag.*, July 2017, San Diego, CA, USA, pp. 1689–1690.

[6] T. Björninen *et al.*, "Development and validation of an equivalent circuit model for UHF RFID IC based on wireless tag measurements," AMTA Symp., 2012, Bellevue, WA, USA, pp. 6.

[7] A. Drossos, *et al.*, "The dependence of electromagnetic energy absorption upon human head tissue composition in the frequency range of 300-3000 MHz," *IEEE Trans. Microwave Theory and Techn.*, vol. 48, no. 11, pp. 1988–1995, Nov. 2000.

[8] A. N. Bashkatov, V. V. Tuchin, *et al.*, "Glucose and mannitol diffusion in human dura mater," *Biophys. J.*, Nov. 2003.

[9] S. Gabriel *et al.*, "The dielectric properties of biological tissues: III. Parametric models for the dielectric spectrum of tissues," *Phys. Med. Biol.*, vol. 41, no. 11, pp. 2271–2293, Nov. 1996.

[10] IT'IS Fondation, Tissue Properties [Online]. Available: https://www.itis.ethz.ch/virtual-population/tissue-properties/downloads

[11] David L. Means *et al.*, "Evaluating compliance with FCC guidelines for human exposure to radiofrequency electromagnetic fields," *Supplement C to OET Bulletin 65*, Washington, DC, 1997.

[12] J. Virkki *et al.*,"The effects of recurrent stretching on the performance of electro-textile and screen-printed ultra-high-frequency radio-frequency identification tags," *Text. Res. J.*, vol. 85, no. 3, pp. 294–301, Aug. 2015.